

# Particle growth behavior of carbon-supported Pt, Ru, PtRu catalysts prepared by an impregnation reductive-pyrolysis method for direct methanol fuel cell anodes

Tomoyuki Kawaguchi, Wataru Sugimoto\*, Yasushi Murakami, Yoshio Takasu

*Department of Fine Materials Engineering, Faculty of Textile Science and Technology, Shinshu University, 3-15-1 Tokida, Ueda 386-8567, Japan*

Received 5 August 2004; revised 22 October 2004; accepted 25 October 2004

Available online 8 December 2004

## Abstract

Carbon-supported Pt, Ru, and binary PtRu catalysts were prepared by an impregnation-reductive pyrolysis method at various temperatures, with  $\text{Pt}(\text{NH}_3)_2(\text{NO}_2)_2$  and  $\text{Ru}(\text{NO}_3)_3$  as precursors. The effect of the reductive pyrolysis temperature on the structure of the metal particles and its relationship to the electrocatalytic activity toward methanol and preadsorbed carbon monoxide ( $\text{CO}_{\text{ad}}$ ) oxidation was examined. The decomposition temperature of the  $\text{Pt}_{50}\text{Ru}_{50}$  mixed precursor shifted to a temperature lower than that of the Ru single-source precursor. High-resolution scanning electron microscopy, X-ray diffraction, and  $\text{CO}_{\text{ad}}$  stripping voltammetry of Pt/C and Ru/C indicated that Ru nanoparticles tend to grow drastically when the pyrolysis temperature is increased, whereas Pt nanoparticles are more resistant to particle growth. Scanning transmission electron microscopy coupled with energy-dispersive X-ray spectroscopy analysis showed that there is a slight compositional variation between individual nanoparticles, depending on the particle size. The  $\text{Pt}_{50}\text{Ru}_{50}/\text{C}$  catalyst prepared at 200 °C exhibited the maximum electrocatalytic activity toward methanol oxidation per mass of PtRu, which is discussed based on the appropriate balance of precursor decomposition and particle growth.

© 2004 Elsevier Inc. All rights reserved.

**Keywords:** Direct methanol fuel cells; Anode catalysts; PtRu; Alloys; Carbon monoxide oxidation; CO stripping voltammetry; Chronoamperometry; STEM-EDX

## 1. Introduction

Because of the comparatively low operation temperature of the direct methanol fuel cell (DMFC), poisoning of the anode catalyst by carbon monoxide becomes a major problem. Therefore, the material design of highly active electrocatalysts is an important subject in DMFC development. High-surface-area PtRu alloy supported on carbon black is one of the most promising materials as an anode catalyst for DMFC [1–21] because of its high tolerance for carbon monoxide poisoning. The promotion effect of Ru has mainly been discussed based on the so-called bifunctional mechanism [4–6, 22–42] or ligand effect [36–50] or a mixture of both.

The fundamental properties of the methanol oxidation reaction have been well established with the use of well-defined catalysts, such as Ru-decorated single crystals, model electrocatalysts, and bulk alloys. In contrast, understanding the relationship between the physical and electrocatalytic properties of PtRu nanoparticles supported on carbon black is not as straightforward. Composition, particle size, and dispersion state and their delicate control are only a few of the requirements for practical catalysts. The co-impregnation method [14–19, 51–60] is a simple and effective method for the preparation of high-surface-area carbon-supported electrocatalysts. We have shown that the structural properties and electrocatalysis of carbon-supported PtRu nanoparticles vary with the type of precursor employed, and the activity toward methanol electro-oxidation is sensitive to the pyrolysis temperature [14]. In our previous study, we reported the effect of the type of precursor at pyrolysis tem-

\* Corresponding author. Fax: +81 268 22 9048.

E-mail address: [wsugi@shinshu-u.ac.jp](mailto:wsugi@shinshu-u.ac.jp) (W. Sugimoto).

peratures between 150 and 550 °C. Reductive pyrolysis at 200 °C was preferable for highly active catalysts. For a better understanding of the effect of the pyrolysis temperature on the nanostructure and electrocatalysis of PtRu/C, a systematic study of the nanometer scale is necessary.

Here we report the process of particle growth of Pt, Ru, and PtRu catalysts supported on carbon as a function of the pyrolysis temperature up to 800 °C. Emphasis was placed on the difference in the particle growth behavior of Pt, Ru, and PtRu and the composition variation between individual PtRu nanoparticles. The activity toward methanol and preadsorbed carbon monoxide oxidation of Pt<sub>50</sub>Ru<sub>50</sub>/C were examined and discussed based on the difference in the structure of the nanoparticles.

## 2. Experimental

Pt/C, Ru/C, and Pt<sub>50</sub>Ru<sub>50</sub>/C (30 mass% metal) catalysts were prepared by a conventional impregnation method reported previously [14]. The catalysts were prepared by the introduction of appropriate amounts of carbon black (Vulcan XC-72R) into ethanolic solutions of Pt(NH<sub>3</sub>)<sub>2</sub>(NO<sub>2</sub>)<sub>2</sub> (Ishifuku Metal Industry), Ru(NO<sub>3</sub>)<sub>3</sub> (Tanaka Kikinzoku Kogyo K.K.), or a 1:1 molar ratio of Pt(NH<sub>3</sub>)<sub>2</sub>(NO<sub>2</sub>)<sub>2</sub> and Ru(NO<sub>3</sub>)<sub>3</sub>. For the Pt source, 4 mM ( $M = \text{mol dm}^{-3}$ ) Pt(NH<sub>3</sub>)<sub>2</sub>(NO<sub>2</sub>)<sub>2</sub> dissolved in ethanol was used. An ethanolic solution of 4 mM Ru(NO<sub>3</sub>)<sub>3</sub> was used as the Ru source. After thorough mixing, the precursor solution was allowed to dry at 60 °C to a powder. The dried powder was then reduced in a tube furnace under flowing H<sub>2</sub> (10%) + N<sub>2</sub> (90%) gas for 2 h at various temperatures.

The pyrolysis process of the precursor powders was investigated by thermogravimetry (TG, Shimadzu TGA-50) under a constant flow of H<sub>2</sub> (10%) + N<sub>2</sub> (90%) at a heating rate of 5 °C min<sup>-1</sup>. The structure of Pt/C, Ru/C, and Pt<sub>50</sub>Ru<sub>50</sub>/C was characterized by X-ray diffraction (XRD) (Rigaku RINT-2550 with monochromated Cu-K $\alpha$  radiation), high-resolution scanning electron microscopy (HR-SEM) (Hitachi S-5000), high-resolution scanning transmission electron microscopy (HR-STEM) (Hitachi HF-2210), and energy-dispersive X-ray spectroscopy (EDX) (Noran Instruments Voyager). Scanning transmission electron microscopy coupled with energy-dispersive X-ray spectroscopy (STEM-EDX) was utilized to analyze the single-particle composition of PtRu.

Electrochemical studies were conducted with a three-electrode-type beaker cell equipped with a platinum mesh counter electrode, an Ag/AgCl reference electrode, and the working electrode. A Luggin capillary faced the working electrode at a distance of 2 mm. The working electrodes were prepared by the thin-film electrode method [61]. Briefly, 20 mg of the catalyst powder was dispersed in 10 mL of methanol and was subjected to ultrasonication for 30 min. Then, 20  $\mu\text{L}$  of the catalyst powder dispersion (40  $\mu\text{g}$  of the catalyst powder containing 12  $\mu\text{g}$  of metal) was

dropped on a mirror-polished Glassy Carbon (Tokai Carbon Co., Ltd.) substrate (grade 20SS, 5 mm in diameter). After drying at 60 °C, 20  $\mu\text{L}$  of a 1 wt% Nafion (R) alcoholic solution was also dropped on the electrode surface to stabilize the electrocatalysts on the Glassy Carbon rod surface. All potentials throughout this paper are given in the reversible hydrogen electrode (RHE) scale. The electrocatalytic oxidation of preadsorbed carbon monoxide (CO<sub>ad</sub>) was measured by CO<sub>ad</sub> stripping voltammetry at a scan rate of 10 mV s<sup>-1</sup>. CO gas was passed into the cell (0.5 M H<sub>2</sub>SO<sub>4</sub>, 60 °C) for 40 min to allow adsorption of CO to the accessible metal surface while maintaining a constant voltage of 270 mV vs RHE. Excess CO was purged with N<sub>2</sub> gas for 40 min. The amount of CO<sub>ad</sub> was evaluated by integration of the CO<sub>ad</sub> stripping peak, corrected for the electric double-layer capacitance. The electrochemical oxidation of methanol was characterized by the quasi-steady-state current density at 470 mV vs RHE in 1.0 M CH<sub>3</sub>OH + 0.5 M H<sub>2</sub>SO<sub>4</sub> solution. All electrochemical measurements were carried out at 60 °C.

## 3. Results and discussion

### 3.1. Carbon-supported platinum

The pyrolysis process in H<sub>2</sub> (10%) + N<sub>2</sub> (90%) for the Pt/C precursor powder is shown in Fig. 1a. The decomposition of the Pt/C precursor was completed at about 170 °C. HR-SEM images of Pt/C pyrolyzed at various temperatures are shown in Fig. 2. The histograms of the particle size estimated from 100 particles as a function of the pyrolysis temperature are shown in Fig. 3. More than 80% of the Pt particles were in the range of 2–5 nm, irrespective of the pyrolysis temperature. The relative abundance of small particles (< 3 nm) decreased with increasing pyrolysis temperatures (200 °C, 28%; 450 °C, 12%; 800 °C, 8%), whereas that of particles in the range of 3–4 nm increased slightly with increasing pyrolysis temperature (200 °C, 33%; 450 °C,

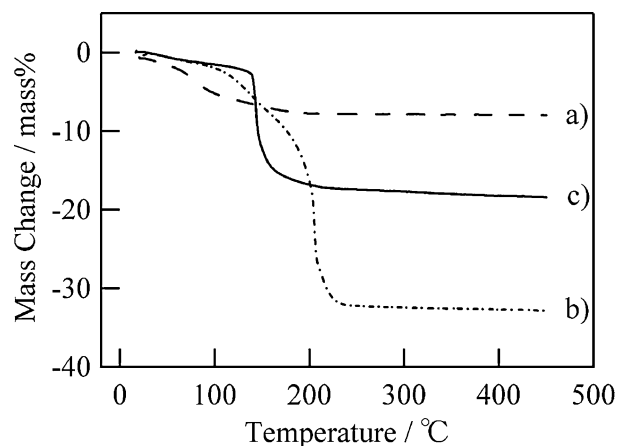


Fig. 1. The TG curves: (a) Pt(NH<sub>3</sub>)<sub>2</sub>(NO<sub>2</sub>)<sub>2</sub>, (b) Ru(NO<sub>3</sub>)<sub>3</sub>, and (c) Pt(NH<sub>3</sub>)<sub>2</sub>(NO<sub>2</sub>)<sub>2</sub> + Ru(NO<sub>3</sub>)<sub>3</sub>, supported on Vulcan XC-72R carbon black powder under flowing H<sub>2</sub>(10%)–N<sub>2</sub>(90%).

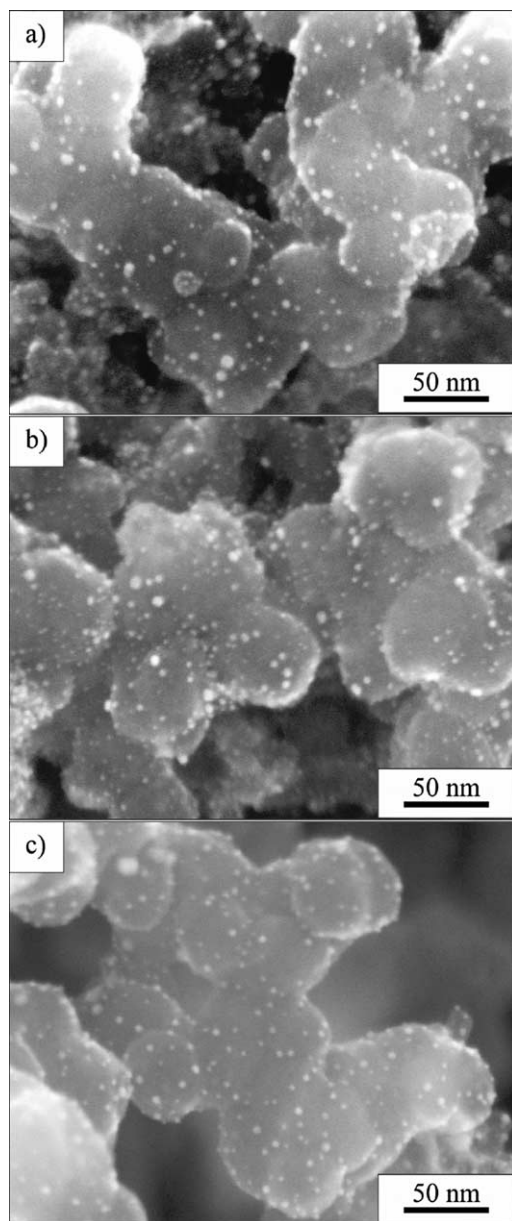


Fig. 2. HR-SEM images of Pt/C pyrolyzed under reducing condition at (a) 200, (b) 450, and (c) 800 °C.

45%; 800 °C, 50%). The relative abundance of larger particles ( $> 4$  nm) was not significantly affected by the pyrolysis temperature (200 °C, 39%; 450 °C, 43%; 800 °C, 42%). The XRD patterns of Pt/C pyrolyzed at various temperatures are shown in Fig. 4. The XRD patterns could be indexed based on the fcc structure of Pt metal. The sharpening of the XRD peaks indicates an increase in the average crystallite size with increasing temperature of pyrolysis.

$\text{CO}_{\text{ad}}$  stripping voltammograms for Pt/C are shown in Fig. 5. The peak of the  $\text{CO}_{\text{ad}}$  oxidation appeared at 670 mV vs RHE. The mean particle size of Pt calculated from the electrochemically active surface area increased slightly with increasing pyrolysis temperature; 2.5, 2.9, and 3.4 nm for the products pyrolyzed at 200, 450, and 800 °C, respectively.

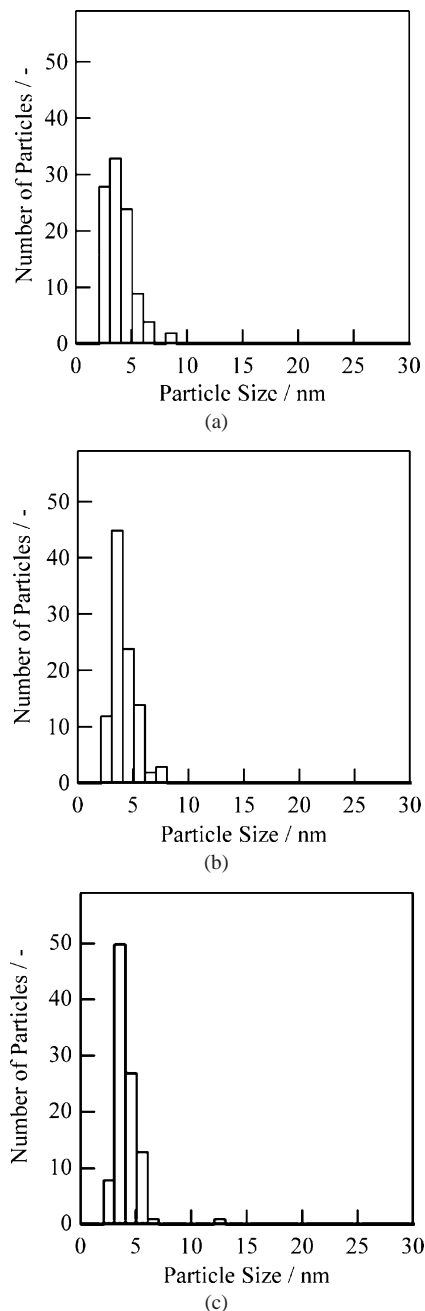


Fig. 3. Histograms of Pt/C pyrolyzed under reducing condition at (a) 200, (b) 450, and (c) 800 °C.

This observation is consistent with the sharpening of the XRD peak, suggesting an increase in crystallite size, which is particularly notable for the product pyrolyzed at 800 °C.

### 3.2. Carbon-supported ruthenium

The decomposition of the Ru/C precursor powder was completed at about 250 °C (Fig. 1b), which is 80 °C higher than the corresponding temperature observed for Pt/C precursor (Fig. 1a). HR-SEM images of Ru/C pyrolyzed at various temperatures are shown in Fig. 6. The particle size distribution at different pyrolysis temperatures is shown in Fig. 7.

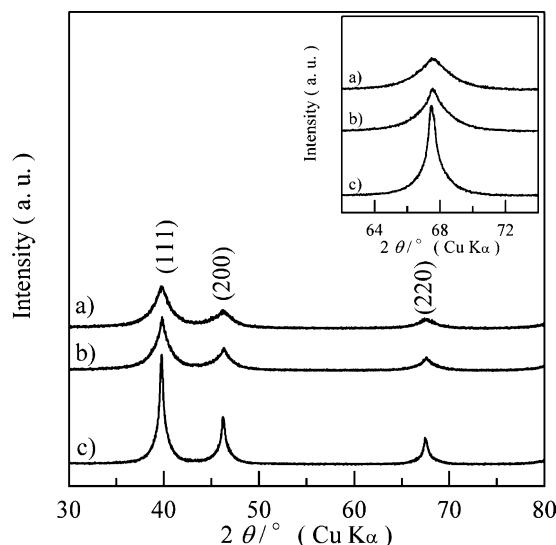


Fig. 4. The XRD patterns of Pt/C pyrolyzed under reducing condition at (a) 200, (b) 450, and (c) 800 °C.

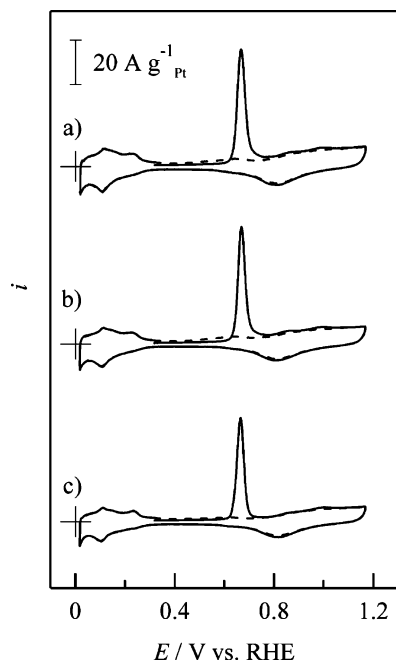


Fig. 5. The  $\text{CO}_{\text{ad}}$ -stripping voltammograms at  $10 \text{ mV s}^{-1}$  of Pt/C pyrolyzed at (a) 200, (b) 450, and (c) 800 °C in  $0.5 \text{ M H}_2\text{SO}_4$  (60 °C).

In contrast to Pt/C, Ru particles clearly showed a tendency to grow with increasing temperature of pyrolysis. The relative abundance of particles larger than 4 nm significantly increased with increasing pyrolysis temperature (200 °C, 7%; 450 °C, 39%; 800 °C, 62%). As shown in Fig. 6c, Ru particles as large as 30 nm (marked with arrows) were observed in addition to the smaller particles (2 nm) for the Ru/C catalyst prepared at 800 °C.

The XRD patterns for Ru/C pyrolyzed at various temperatures are shown in Fig. 8. The XRD patterns could be indexed based on the hcp structure of Ru metal. The sharpening of the XRD peaks indicates an increase in the aver-

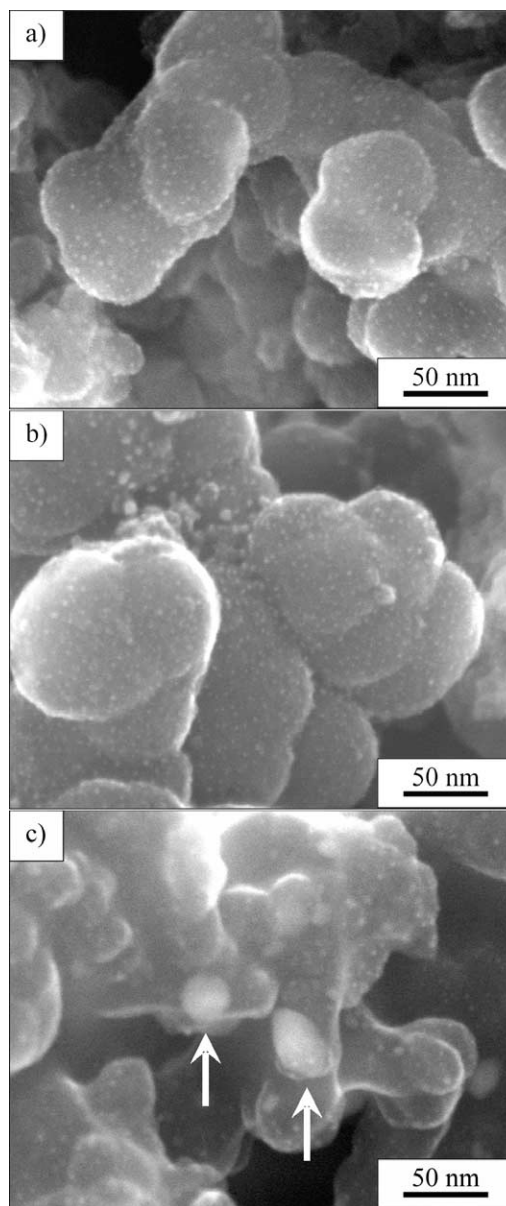


Fig. 6. HR-SEM images of Ru/C pyrolyzed under reducing condition at (a) 200, (b) 450, and (c) 800 °C.

age crystallite size with increasing temperature of pyrolysis. The sharpening of the peaks was more apparent for Ru/C compared with Pt/C, consistent with the HR-SEM analysis revealing an increase in particle size.

The  $\text{CO}_{\text{ad}}$  stripping voltammograms of Ru/C pyrolyzed at various temperatures are shown in Fig. 9. The peak of the  $\text{CO}_{\text{ad}}$  oxidation appeared at 450–480 mV vs RHE on Ru/C. The  $\text{CO}_{\text{ad}}$  oxidation charge decreased drastically with increasing pyrolysis temperature. Quantitative evaluation of the electrochemically active surface from  $\text{CO}_{\text{ad}}$  stripping voltammetry for Ru/C is complicated [19] and is strongly dependent on the measuring conditions, such as preadsorption potential and operating temperature. Here we have not optimized the preadsorption potential; thus only a semi-quantitative assessment can be discussed, and the discussion

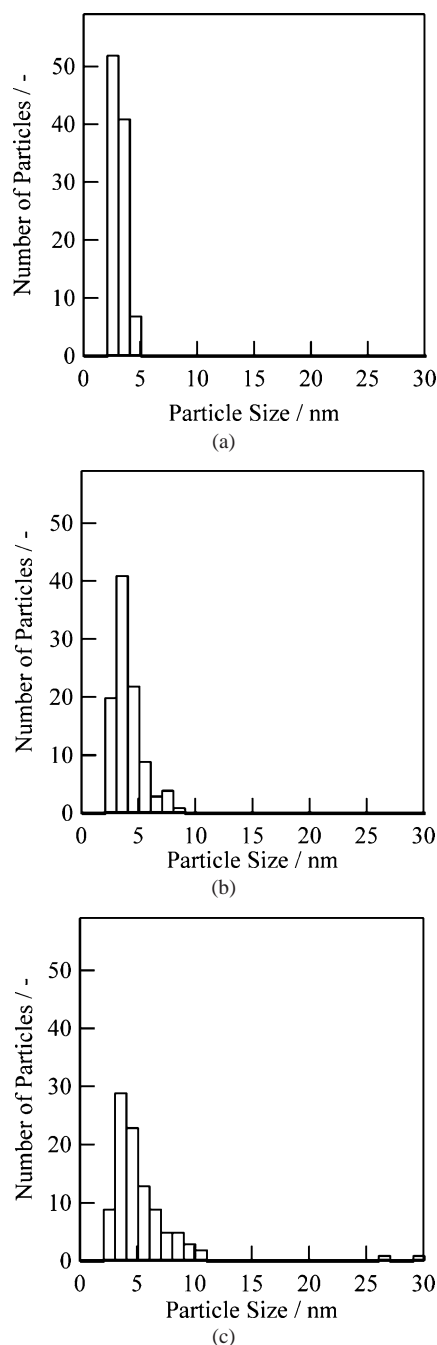


Fig. 7. Histograms of Ru/C pyrolyzed under reducing condition at (a) 200, (b) 450, and (c) 800 °C.

of the  $\text{CO}_{\text{ad}}$  oxidation on Ru/C will be confined to the relative change in the amount of adsorbed CO. The  $\text{CO}_{\text{ad}}$  oxidation charge for Ru/C pyrolyzed at 800 °C was only 21% of the value for Ru/C pyrolyzed at 200 °C. The decrease in the electrochemically active surface area with increasing pyrolysis temperature for Ru/C was much more profound compared with Pt/C. These results are consistent with the particle size analysis of Pt/C and Ru/C by HR-SEM and XRD. The particle growth behavior of the Ru particles is more significant than that of the Pt particles. The difference in the particle growth behavior of Pt and Ru particles is prob-

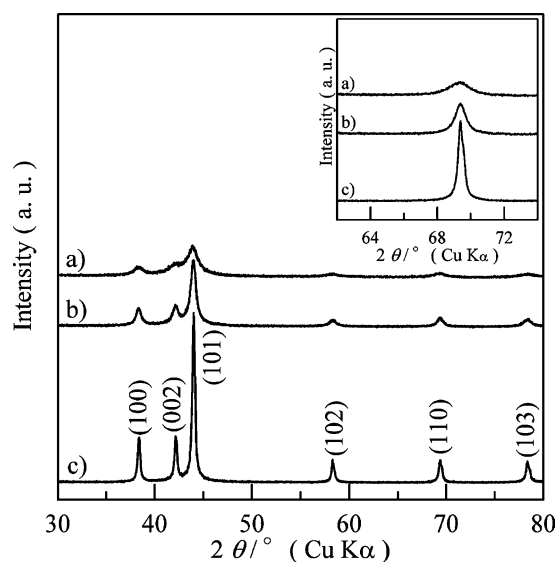


Fig. 8. The XRD patterns of Ru/C pyrolyzed under reducing condition at (a) 200, (b) 450, and (c) 800 °C.

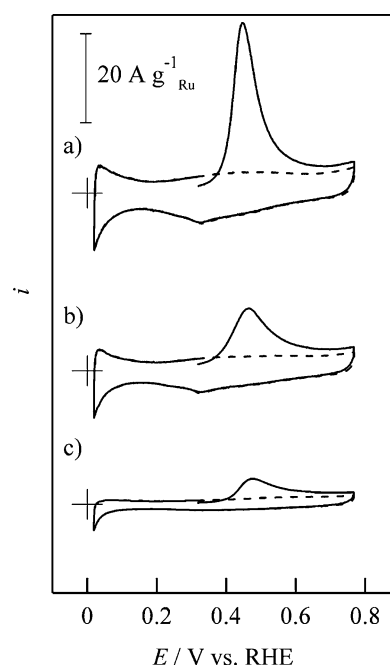


Fig. 9. The  $\text{CO}_{\text{ad}}$ -stripping voltammograms at  $10 \text{ mV s}^{-1}$  of Ru/C pyrolyzed at (a) 200, (b) 450, and (c) 800 °C in  $0.5 \text{ M H}_2\text{SO}_4$  (60 °C).

ably due to differences in physical properties between Pt and Ru (for example, interaction with hydrogen, surface free energy, interaction with the carbon support, etc.).

### 3.3. Carbon-supported $\text{Pt}_{50}\text{Ru}_{50}$

The decomposition of the binary  $\text{Pt}_{50}\text{Ru}_{50}/\text{C}$  precursor was completed at 200 °C (Fig. 1c). In the case of the PtRu mixed precursor, the Pt precursor and the Ru precursor decomposed simultaneously in a single process. The decomposition temperature of the PtRu mixed precursor was lower



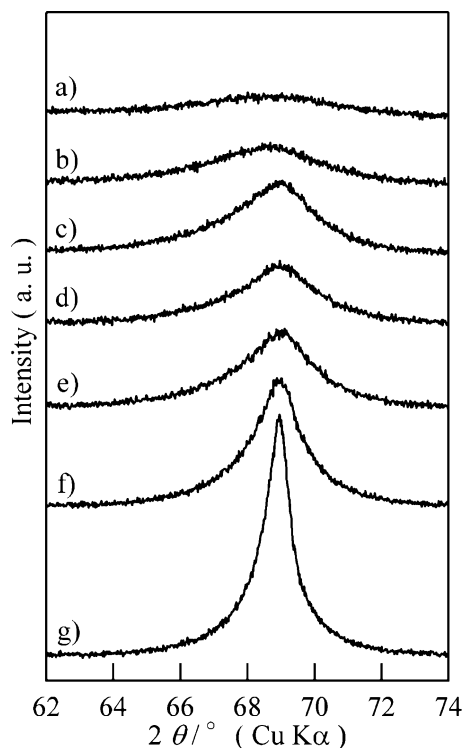


Fig. 10. The XRD patterns of Pt<sub>50</sub>Ru<sub>50</sub>/C catalysts prepared at (a) 150, (b) 200, (c) 300, (d) 450, (e) 500, (f) 600, and (g) 800 °C.

than that of the Ru single-source precursor (Fig. 1b). These facts suggest that the Pt and Ru sources were mixed at an atomic level in the precursor solution. The single-step decomposition process of the PtRu mixed precursor is preferable from the standpoint of bimetal alloying, since nucleation of the two metals will occur simultaneously.

Fig. 10 shows the XRD patterns of Pt<sub>50</sub>Ru<sub>50</sub>/C pyrolyzed at various temperatures. The XRD peak sharpened with increasing pyrolysis temperature, especially above 600 °C, suggesting an increase in the particle size and/or an increase in crystallinity. With increasing pyrolysis temperature from 150 to 450 °C, the fcc(220) peak shifted to higher reflection angles, suggesting that greater amounts of Ru were introduced into the fcc structure.

STEM images of Pt<sub>50</sub>Ru<sub>50</sub>/C prepared at 200, 450, and 800 °C are shown in Fig. 11. The average bulk Ru content obtained by EDX analysis was in accord with the nominal contents, Pt:Ru = 45:55, 51:49, 48:52 Ru mol% at 200, 450, and 800 °C, respectively. The Ru content of individual particles with different particle sizes is shown in Fig. 12, along with the relative abundance as a function of the pyrolysis temperature. Approximately 70–80% of the measured particles were in the range of 2–5 nm for the catalysts, irrespective of the pyrolysis temperature. The majority of the alloy particles (80% or more) in the Pt<sub>50</sub>Ru<sub>50</sub>/C catalysts prepared at 200 to 450 °C is in the range of 2–5 nm, in accordance with our previous results [14]. The Ru contents for these individual particles were close to unity. For particles less than 2 nm or more than 5 nm in diameter (about

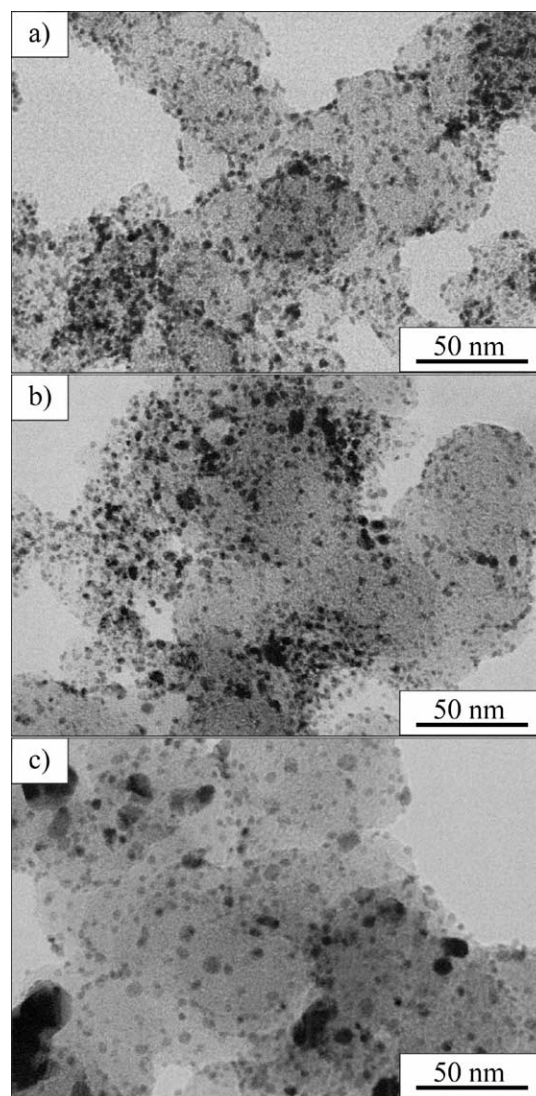


Fig. 11. The STEM images of Pt<sub>50</sub>Ru<sub>50</sub>/C catalysts pyrolyzed at (a) 200, (b) 450, and (c) 800 °C.

20–30% of all measured particles), the Ru content tended to deviate from the nominal content. The histogram also shows that the relative abundance of relatively large particles (> 5 nm) increased with increasing pyrolysis temperatures (200 °C, 3%; 450 °C, 20%; 800 °C, 26%), which is consistent with the XRD results. In particular, PtRu particles larger than 30 nm were observed when the pyrolysis temperature was 800 °C (Fig. 11c), indicating that the high-temperature particle growth behavior of PtRu particles is similar to that of Ru particles. That is, PtRu particles tend to sinter at high temperature.

The CO<sub>ad</sub> stripping voltammograms for Pt<sub>50</sub>Ru<sub>50</sub>/C pyrolyzed at various temperatures are shown in Fig. 13. The peak of the CO<sub>ad</sub> oxidation appeared at 450–465 mV vs RHE. Similar to the behavior of Ru/C and Pt/C, the CO<sub>ad</sub> oxidation charge decreased for Pt<sub>50</sub>Ru<sub>50</sub>/C with increasing pyrolysis temperatures. In addition, an oxidation shoulder peak is observed near 600 mV vs RHE. These peaks are at-

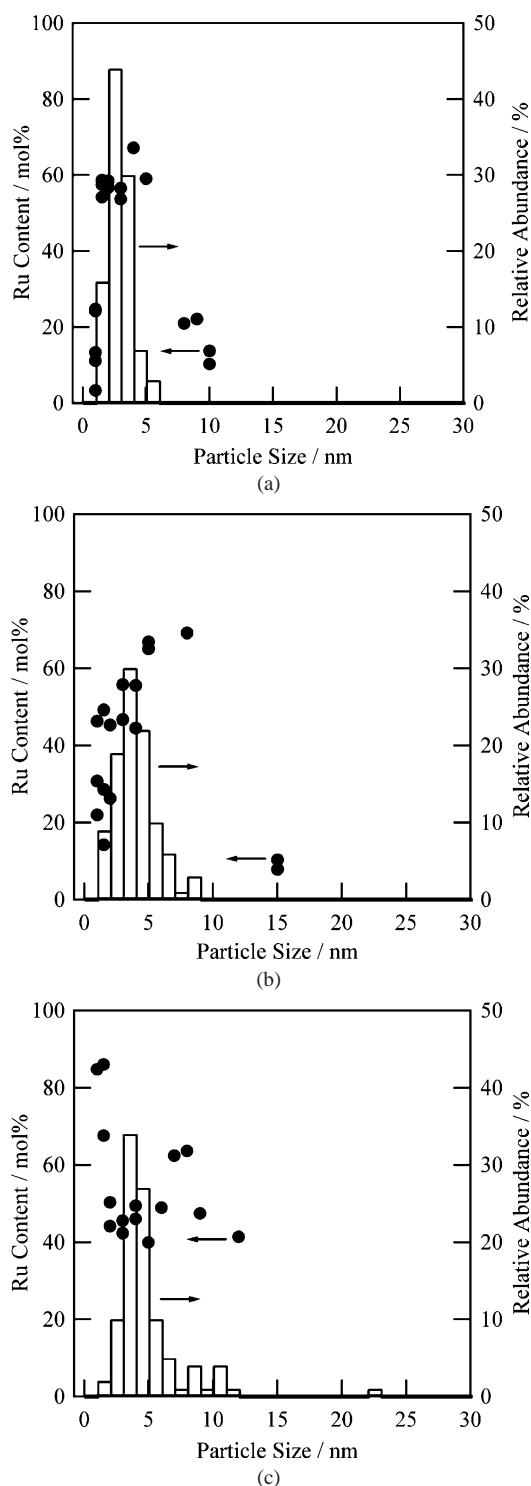


Fig. 12. The Ru contents of individual particles in Pt<sub>50</sub>Ru<sub>50</sub>/C pyrolyzed under reducing condition at (a) 200, (b) 450, and (c) 800 °C (left axis) and the relative abundance as a function of the particle size (right axis) estimated from STEM-EDX analysis.

tributed to the CO<sub>ad</sub> oxidation on Pt or Pt-rich surfaces, since the electrode potentials are close to that of Pt/C (see Fig. 5) [19].

The effect of the pyrolysis temperature on the electrocatalytic activity for methanol oxidation is shown in Fig. 14.

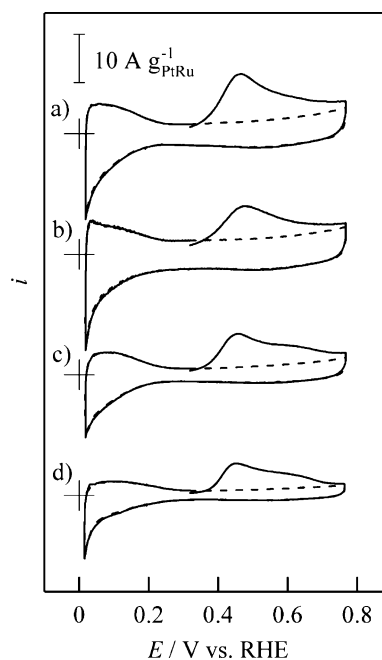


Fig. 13. The CO<sub>ad</sub>-stripping voltammograms at 10 mV s<sup>-1</sup> of Pt<sub>50</sub>Ru<sub>50</sub>/C catalysts pyrolyzed at (a) 150, (b) 200, (c) 450, and (d) 800 °C in 0.5 M H<sub>2</sub>SO<sub>4</sub> (60 °C).

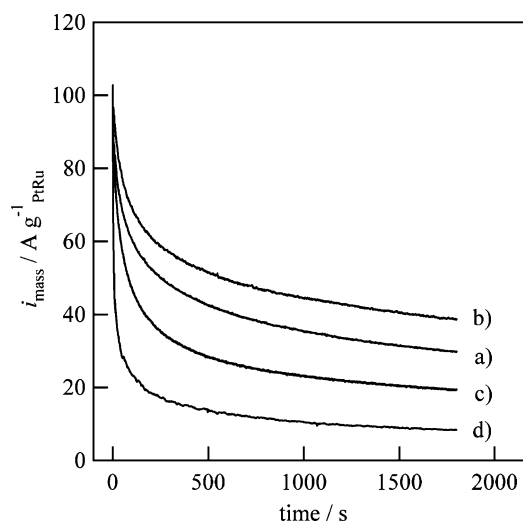


Fig. 14. The methanol oxidation current density as a function of measurement time for Pt<sub>50</sub>Ru<sub>50</sub>/C catalysts pyrolyzed at (a) 150, (b) 200, (c) 450, and (d) 800 °C in 0.5 M H<sub>2</sub>SO<sub>4</sub> + 1 M CH<sub>3</sub>OH at 60 °C at 470 mV vs RHE.

The sample pyrolyzed at 200 °C exhibited the highest current density with 42 A g<sup>-1</sup> PtRu. Although the alloying of ruthenium with platinum progresses as the pyrolysis temperature is increased, large particles are also generated with increasing pyrolysis temperature. Such features reduce the mass activity for methanol oxidation. In addition, if there are Pt-rich particles on the surface, these may also contribute to the decrease in activity [7]. The low activity of the catalyst pyrolyzed at 150 °C is most likely due to the incomplete decomposition of the PtRu precursor (Fig. 1c).

The decomposition of the PtRu precursor occurs in the range from 150 to 200 °C. If the precursor is not completely reduced to the metal state, residual organics should hinder the electrocatalytic activity. This can be seen in the cyclic voltammograms (Fig. 13), which show that the electrocatalyst pyrolyzed at 150 °C tends to have a smaller electric double-layer capacitance. This is suggestive of a low electrochemically active surface area owing to the residual species covering the electrocatalyst surface. The catalyst preparation should be around 200 °C where sintering is inhibited and a good dispersion state as well as good alloying state of the Pt<sub>50</sub>Ru<sub>50</sub> nanoparticles are achieved.

Particle growth is one of the causes of catalyst activity degradation in an operating fuel cell. There may be some similarities between the high-temperature particle growth process observed in this study and the catalyst activity degradation process in a practical fuel cell. The present results for the particle growth behavior of PtRu particles at high temperature may give insights into the catalyst degradation process in actual fuel cells.

#### 4. Conclusions

The structures of Pt, Ru, and Pt<sub>50</sub>Ru<sub>50</sub> nanoparticles supported on carbon and their relationship to the electrocatalytic activity toward CO<sub>ad</sub> and methanol oxidation were examined. HR-SEM analysis, XRD, and CO<sub>ad</sub> stripping voltammetry showed that the particle size drastically increased with increasing pyrolysis temperature for Ru/C catalyst, in contrast to Pt/C. Analysis of the size and composition of individual Pt<sub>50</sub>Ru<sub>50</sub> nanoparticles by STEM-EDX showed that 70–80% of the nanoparticles had a size of 2–5 nm and a composition close to unity. The highest mass activity of the Pt<sub>50</sub>Ru<sub>50</sub>/C prepared at 200 °C was suggested to be a result of the suitable balance between the sintering state, dispersion state, and alloying state.

#### Acknowledgments

The authors are grateful to Ishifuku Metal Industry Co. for kindly supplying Pt(NH<sub>3</sub>)<sub>2</sub>(NO<sub>2</sub>)<sub>2</sub>. This work was supported in part by the Polymer Electrolyte Fuel Cell Program of the New Energy and Industrial Technology Development Organization (NEDO) of Japan, in collaboration with Toray Industries, Inc., and the MEXT 21st Century COE Program of Japan.

#### References

- [1] M. Hogarth, T. Ralph, *Platinum Met. Rev.* 46 (2002) 146.
- [2] A.S. Aricò, Srinivasan, V. Antonucci, *Fuel Cells* 1 (2001) 1.
- [3] J.O'M. Bockris, H. Wroblowa, *J. Electroanal. Chem.* 7 (1964) 428.
- [4] M. Watanabe, S. Motoo, *J. Electroanal. Chem.* 60 (1975) 267.
- [5] M. Watanabe, S. Motoo, *J. Electroanal. Chem.* 60 (1975) 275.
- [6] H.N. Dinh, X. Ren, F.H. Garzon, P. Zelenay, S. Gottesfeld, *J. Electroanal. Chem.* 491 (2000) 222.
- [7] B.D. McNicol, R.T. Short, *J. Electroanal. Chem.* 81 (1977) 249.
- [8] J.B. Goodenough, A. Hamnett, B.J. Kennedy, R. Manoharan, S.A. Weeks, *J. Electroanal. Chem.* 240 (1988) 133.
- [9] A. Hamnett, S.A. Weeks, B.J. Kennedy, G. Troughton, P.A. Christensen, *Ber. Bunsen-Ges. Phys. Chem.* 94 (1990) 1014.
- [10] A.S. Aricò, P. Creti, H. Kim, R. Mantegna, N. Giordano, V. Antonucci, *J. Electrochem. Soc.* 143 (1996) 3950.
- [11] A.S. Aricò, A.K. Shukla, K.M. El-Khatib, P. Creti, V. Antonucci, *J. Appl. Electrochem.* 29 (1999) 671.
- [12] T.J. Schmidt, H.A. Gasteiger, R.J. Behm, *Electrochem. Commun.* 1 (1999) 1.
- [13] A.S. Aricò, P. Creti, E. Modica, G. Monforte, V. Baglio, V. Antonucci, *Electrochim. Acta* 45 (2000) 4319.
- [14] Y. Takasu, T. Fujiwara, Y. Murakami, K. Sasaki, M. Oguri, T. Asaki, W. Sugimoto, *J. Electrochem. Soc.* 147 (2000) 4421.
- [15] Y. Takasu, H. Itaya, T. Iwazaki, R. Miyoshi, T. Ohnuma, W. Sugimoto, Y. Murakami, *Chem. Commun.* 2001 (2001) 341.
- [16] Y. Takasu, T. Kawaguchi, W. Sugimoto, Y. Murakami, *Electrochim. Acta* 48 (2003) 3861.
- [17] Y. Takasu, W. Sugimoto, Y. Murakami, *Catal. Surv. Asia* 7 (2003) 21.
- [18] Y. Takasu, H. Itaya, T. Kawaguchi, W. Sugimoto, Y. Murakami, *Stud. Surf. Sci. Catal.* 145 (2003) 279.
- [19] T. Kawaguchi, W. Sugimoto, Y. Murakami, Y. Takasu, *Electrochem. Commun.* 6 (2004) 480.
- [20] A.V. Tripković, K.D. Popović, B.N. Grgur, B. Blizanac, P.N. Ross, N.M. Markovic, *Electrochim. Acta* 47 (2002) 3707.
- [21] C. Roth, N. Martz, F. Hahn, J.-M. Léger, C. Lamy, H. Fuess, *J. Electrochem. Soc.* 149 (2002) E433.
- [22] M. Watanabe, S. Motoo, *Denki Kagaku* 41 (1973) 190 (presently *Electrochemistry*).
- [23] T. Yajima, H. Uchida, M. Watanabe, *J. Phys. Chem. B* 108 (2004) 2654.
- [24] E. Ticanelli, J.G. Beery, M.T. Paffett, S. Gottesfeld, *J. Electroanal. Chem.* 258 (1989) 61.
- [25] X. Ren, P. Zelenay, S. Thomas, J. Davey, S. Gottesfeld, *J. Power Sources* 86 (2000) 111.
- [26] H.A. Gasteiger, N. Markovic, P.N. Ross Jr., E.J. Cairns, *J. Phys. Chem.* 98 (1994) 617.
- [27] H.A. Gasteiger, N. Markovic, P.N. Ross Jr., E.J. Cairns, *J. Electrochem. Soc.* 141 (1994) 1795.
- [28] H.A. Gasteiger, N. Markovic, P.N. Ross Jr., E.J. Cairns, *Electrochim. Acta* 39 (1994) 1825.
- [29] H.A. Gasteiger, N.M. Markovic, P.N. Ross Jr., *J. Phys. Chem.* 99 (1995) 8290.
- [30] H.A. Gasteiger, N.M. Markovic, P.N. Ross Jr., *J. Phys. Chem.* 99 (1995) 16757.
- [31] S. Swathirajan, Y.M. Mikhail, *J. Electrochem. Soc.* 138 (1991) 1321.
- [32] J. Munk, P.A. Christensen, A. Hamnett, E. Skou, *J. Electroanal. Chem.* 401 (1996) 215.
- [33] H. Wang, C. Wingender, H. Baltruschat, M. Lopez, M.T. Reetz, *J. Electroanal. Chem.* 509 (2001) 163.
- [34] L. Giorgi, A. Pozio, C. Bracchini, R. Giorgi, S. Turtu, *J. Appl. Electrochem.* 31 (2001) 325.
- [35] A.S. Aricò, P.L. Antonucci, E. Modica, V. Baglio, H. Kim, V. Antonucci, *Electrochim. Acta* 47 (2002) 3237.
- [36] H.A. Gasteiger, N. Markovic, P.N. Ross Jr., E.J. Cairns, *J. Phys. Chem.* 97 (1993) 12020.
- [37] G. Tremiliosi-Filho, H. Kim, W. Chrzanowski, A. Wieckowski, B. Grzybowski, P. Kulesza, *J. Electroanal. Chem.* 467 (1999) 143.
- [38] P. Waszczuk, A. Wieckowski, P. Zelenay, S. Gottesfeld, C. Coutanceau, J.-M. Léger, C. Lamy, *J. Electroanal. Chem.* 511 (2001) 55.
- [39] P. Waszczuk, G.-Q. Lu, A. Wieckowski, C. Lu, C. Rice, R.I. Masel, *Electrochim. Acta* 47 (2002) 3637.
- [40] J.C. Davies, B.E. Hayden, D.J. Pegg, *Surf. Sci.* 467 (2000) 118.
- [41] M. Watanabe, Y.M. Zhu, H. Uchida, *Electrochemistry* 68 (2000) 244.



- [42] H. Igarashi, T. Fujino, Y. Zhu, H. Uchida, M. Watanabe, *Phys. Chem. Chem. Phys.* 3 (2001) 306.
- [43] T. Iwasita, F.C. Nart, W. Vielstich, *Ber. Bunsen-Ges. Phys. Chem.* 94 (1990) 1030.
- [44] M. Krausa, W. Vielstich, *J. Electroanal. Chem.* 379 (1994) 307.
- [45] W.F. Lin, M.S. Zei, M. Eiswirth, G. Ertl, T. Iwasita, W. Vielstich, *J. Phys. Chem. B* 103 (1999) 6968.
- [46] R. Liu, H. Iddir, Q. Fan, G. Hou, A. Bo, K.L. Ley, E.S. Smotkin, Y.-E. Sung, H. Kim, S. Thomas, A. Wieckowski, *J. Phys. Chem. B* 104 (2000) 3518.
- [47] C. Lu, C. Rice, R.I. Masel, P.K. Babu, P. Waszczuk, H.S. Kim, E. Oldfield, A. Wieckowski, *J. Phys. Chem. B* 106 (2002) 9581.
- [48] T. Frelink, W. Visscher, J.A.R. van Veen, *Surf. Sci.* 335 (1995) 353.
- [49] T. Frelink, W. Visscher, J.A.R. van Veen, *Langmuir* 12 (1996) 3702.
- [50] M.M.P. Janssen, J. Moolhuysen, *Electrochim. Acta* 21 (1976) 869.
- [51] E.S. Steigerwalt, G.A. Deluga, C.M. Lukehart, *J. Phys. Chem. B* 106 (2002) 760.
- [52] E.S. Steigerwalt, G.A. Deluga, D.E. Cliffel, C.M. Lukehart, *J. Phys. Chem. B* 105 (2001) 8097.
- [53] G. Che, B.B. Lakshmi, C.R. Martin, E.R. Fisher, *Langmuir* 15 (1999) 750.
- [54] G. Che, B.B. Lakshmi, E.R. Fisher, C.R. Martin, *Nature* 393 (1998) 346.
- [55] N. Fujiwara, K. Yasuda, T. Ioroi, Z. Siroma, Y. Miyazaki, *Electrochim. Acta* 70 (2002) 988.
- [56] C.W. Hills, M.S. Nashner, A.I. Frenkel, J.R. Shapley, R.G. Nuzzo, *Langmuir* 15 (1999) 690.
- [57] M.S. Nashner, A.I. Frenkel, D. Somerville, C.W. Hills, J.R. Shapley, R.G. Nuzzo, *J. Am. Chem. Soc.* 120 (1998) 8093.
- [58] M.S. Nashner, A.I. Frenkel, D.L. Adler, J.R. Shapley, R.G. Nuzzo, *J. Am. Chem. Soc.* 119 (1997) 7760.
- [59] C.W. Hills, N.H. Mack, R.G. Nuzzo, *J. Phys. Chem. B* 107 (2003) 2626.
- [60] E. Antolini, F. Cardellini, *J. Alloys Compd.* 315 (2001) 118.
- [61] T.J. Schmidt, H.A. Gasteiger, G.D. Stäb, P.M. Urban, D.M. Kolb, R.J. Behm, *J. Electrochem. Soc.* 145 (1998) 2354.